Signaling pathways in cancer: Holland and colleagues review recent developments in targeting pharmacodynamic biomarkers that could utilize PET of signal transduction pathways in cancer and suggest new strategies for optimizing this potential . . . . ***Page 1333***

Axillary uptake in breast cancer: Song and colleagues determine standardized uptake values of metastatic axillary lymph nodes in patients with invasive ductal breast cancer to assess the pretreatment prognostic value of ^{18}F-FDG PET/CT. . . . ***Page 1337***

Colorectal liver metastases and PET/CT: Muralidharan and colleagues look at the predictive utility of metabolic measurements derived from ^{18}F-FDG PET before liver resection and compare this with other prognostic scoring systems. . . ***Page 1345***

PET, PCC/PGL, and genotype: Rischke and colleagues explore the ability of ^{18}F-DOPA PET to detect and stage pheochromocytomas/paragangliomas and ask whether specific genotypes correlate with tracer uptake . . . . . ***Page 1352***

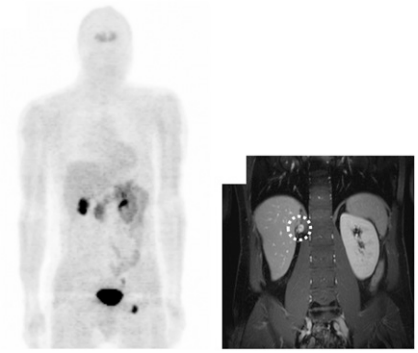

Response to ^{177}Lu-octreotate therapy: van Vliet and colleagues compare the response of bone lesions with that of soft tissues to treatment with ^{177}Lu-octreotate in patients with gastroenteropancreatic and bronchial neuroendocrine tumors. . . . . ***Page 1359***

PET and brain metastases: Galldiks and colleagues investigate the potential of ^{18}F-FET PET for differentiating local recurrent brain metastasis from radiation necrosis after radiation therapy . . . . . ***Page 1367***

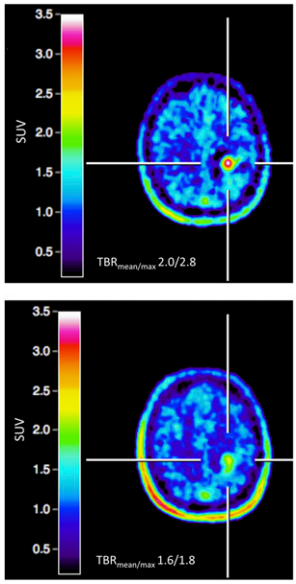

PET for temporal lobectomy: Theodore and colleagues assess the relative value of data from 5-HT$_{1A}$ PET and cerebral metabolic rate of glucose information from ^{18}F-FDG PET for temporal lobectomy planning . . . . . ***Page 1375***

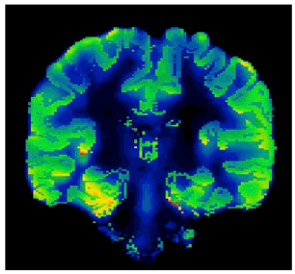

FAA synthesis and lipid incorporation: Pichika and colleagues describe work with a stereoselective synthetic method for ^{19}F-FAA and discuss its potential in PET imaging of human brain arachidonic metabolism in neuroinflammatory disorders such as Alzheimer disease . . ***Page 1383***

Rest–stress functional change: Karimi-Ashtiani and colleagues develop and validate a novel approach for automatic SPECT quantification of rest–stress myocardial motion and thickening changes . . . ***Page 1392***

CZT MPI in obesity: Fiechter and colleagues evaluate the effect of increased body mass on myocardial perfusion imaging quality using a latest-generation γ-camera with cadmium-zinc-telluride semiconductor detectors in patients with high body mass indices . . . . . ***Page 1401***

BAT activity in healthy men: Vrieze and colleagues use ^{18}F-FDG PET/CT to examine the differential effects of an overnight fast and the postprandial state on brown adipose tissue activity . . . . . ***Page 1407***

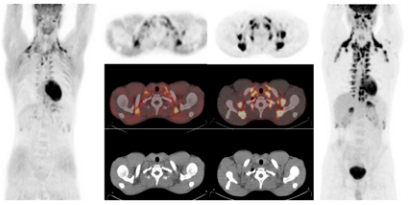

Age effects on serotonin receptors: Matuskey and colleagues use an ^{11}C-labeled tracer and PET to determine whether the availability of brain serotonin receptor 5-HT$_{1B}$ decreases with aging in healthy adults . . . . . ***Page 1411***

PET/MRI workflow: Martinez-Möller and colleagues provide an educational overview of considerations relating to workflow, imaging protocols, and image analysis for

whole-body PET/MRI in oncology, based on early experience with an integrated PET/MRI scanner . . . . . *Page 1415*

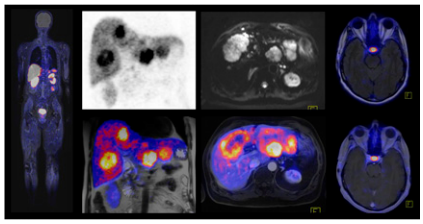

Imaging lymph node metastases: Hall and colleagues develop and compare various dual-labeled monoclonal antibodies against the epithelial cell-adhesion molecule for both noninvasive and intraoperative detection of metastatic lymph nodes in prostate cancer . . . . . *Page 1427*

Positron lymphography: Thorek and colleagues investigate multimodal imaging in animal models using intradermal administration of ^{18}F-FDG for combined diagnostic and intraoperative use, including the use of Cerenkov radiation to optically guide surgical resection of lymph nodes . . . . . *Page 1438*

Site-specific protein radiolabeling: Wållberg and colleagues describe a rapid technique for PET imaging of HER2-positive tumors in less than 1 h using a site-specific ^{11}C-labeled Sel-tagged Affibody molecule. . . . . *Page 1446*

Predosing for ADCs: Boswell and colleagues evaluate in a mouse model a predosing strategy with unconjugated antibody to block antibody–drug conjugate uptake while preserving tumor uptake and efficacy . . . . . *Page 1454*

Amphiphile-encapsulated nanoparticles: Lee and colleagues develop and validate a method for modifying nanoparticles by encapsulation with specific ligand-conjugated amphiphiles and discuss the potential for multimodality and multispecific molecular imaging . . . . . *Page 1462*

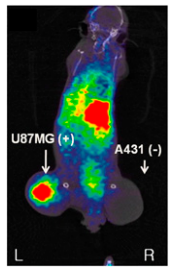

^{18}F-nifene kinetics: Hillmer and colleagues use both kinetic modeling and graphical analysis techniques to analyze the in vivo kinetic properties of this α4β2* nicotinic acetylcholine receptor agonist PET radioligand . . . . . *Page 1471*

Radiometals and sst_2 antagonists: Fani and colleagues explore whether chelated somatostatin antagonists are sensitive to radiometal modifications and look at explanations for this sensitivity . . . . . *Page 1481*

SNMMI/ABNM statement on training: Delbeke and colleagues provide context for and full text of the SNMMI/American Board of Nuclear Medicine joint position statement on optimizing training in nuclear medicine in the era of hybrid imaging. . . . . *Page 1490*

ON THE COVER

This image shows the lymphatics and the main nodal stations in a mouse after injection of ^{18}F-FDG intracutaneously into the tail in a 3-dimensional PET/CT reconstruction.

See page 1440.